JOURNAL OF PLASTIC SURGERY AND HAND SURGERY
2026, VOL. 61, 35–43
https://doi.org/10.2340/jphs.v61.45556

ORIGINAL RESEARCH ARTICLE

Ulnar nerve innervation patterns and muscle fiber type composition of intrinsic hand muscles in mice

Chuxiang Chen[a,b], Mingjie Zhou[a], Chenpei Xu[a], Tingzheng Jiang[a,c], Qianru He[d], Guillaume Prunieres[e], Philippe Liverneaux[f] and Su Jiang[a]*

[a]Department of Hand Surgery, Huashan Hospital, National Health Commission Key Laboratory of Hand Reconstruction, Shanghai Key Laboratory of Peripheral Nerve and Microsurgery, Institute of Hand Surgery, The National Clinical Research Center for Aging and Medicine, Department of Hand and Upper Extremity Surgery, Jing'an District Central Hospital, Fudan University, Shanghai, People's Republic of China; [b]Department of General Surgery, Fengxian District Central Hospital, Shanghai, People's Republic of China; [c]Department of General Practice, Huashan Hospital, Fudan University, Shanghai, People's Republic of China; [d]Department of Pathology, Medical School of Nantong University, Nantong, People's Republic of China; [e]Hand Surgery, Clinic Saint Francois, Haguenau, France; [f]Department of Hand Surgery, Strasbourg University Hospitals, FMTS, ICube CNRS UMR7357, Strasbourg University, Strasbourg, France

ABSTRACT

The motor function of the hand is crucial in daily life, with fine motor abilities relying on intrinsic hand muscles. Ulnar nerve injury causes atrophy of the intrinsic hand muscles it innervates, severely impacting patients' daily activities. However, current understanding of the innervation patterns and muscle fiber composition of these muscles is limited, hindering the development of effective therapies for restoring hand function after such injuries. In this study, we investigated the anatomical basis of ulnar nerve innervation of the lumbrical and interosseous muscles in mice, a common neuromuscular research model. Our findings revealed that the ulnar nerve innervates the third and fourth lumbrical muscles and all interosseous muscles in mice. Six months after median nerve transection, motor endplate (MEP) areas in the ulnar-innervated fourth lumbrical muscle (152.200 ± 10.63 μm^2, $n = 6$) and dorsal interosseous muscles (e.g. third dorsal interosseous muscles: 171.100 ± 10.380 μm^2, $n = 6$) were preserved, whereas MEPs in the median-innervated first and second lumbricals were nearly abolished (e.g. LM1: 16.600 ± 1.126 μm^2, $p < 0.001$, $n = 6$). The third dorsal interosseous muscles predominantly consist of myosin heavy chain (MHC) -I (11.45% ± 1.92%, $n = 6$) and MHC-IIa (88.55% ± 1.92%, $n = 6$) fibers, whereas the lumbrical muscles mainly comprise MHC-IIa (31.67% ± 7.31%, $n = 6$) and MHC-IIb (64.44% ± 7.17%, $n = 6$) fibers. These results provide an essential anatomical and histological foundation for using mice to study the functional recovery of intrinsic hand muscles following ulnar nerve injury.

ARTICLE HISTORY
Received 16 August 2025
Accepted 27 January 2026
Published 16 March 2026

KEYWORDS
Peripheral nerve; ulnar nerve; intrinsic hand muscle; muscle fiber type; neuromuscular junction.

Introduction

Human daily life relies heavily on the use of hands. The dexterity of the hand depends not only on finger flexion and extension, but also on coordinated fine motor actions. These include pinching, abduction, and adduction of the fingers. These fine motor movements are primarily achieved through the contraction and relaxation of multiple intrinsic hand muscles [1, 2]. The intrinsic hand muscles are innervated by the median nerve and the ulnar nerve. Severe trauma, local compression, and other causes can result in ulnar nerve injury. However, compared with injuries to other peripheral nerves in the upper limb, ulnar nerve injury, especially involving the high-level segment, often leads to a poorer prognosis. Due to the long distance required for nerve regeneration, the small size of the intrinsic hand muscles, and their susceptibility to atrophy, even with timely surgical intervention and pharmacological treatment, functional recovery of the intrinsic hand muscles remains limited. This manifests specifically as impaired finger abduction, adduction, and pinching movements, along with the inability to fully extend the ring and little fingers. Consequently, tasks that require precise motor control, such as writing or picking up small objects, become significantly more difficult, which can severely impact a patient's daily life [3, 4]. Improving the function of intrinsic hand muscles after ulnar nerve injury, uncovering deeper underlying mechanisms, and enhancing therapeutic outcomes remain urgent clinical challenges that need to be addressed to minimize the impact on patients' quality of life.

To further understand the innervation of intrinsic hand muscles by the ulnar nerve and explore rehabilitation methods to promote functional recovery after ulnar nerve injury, it is necessary to continuously evaluate various therapeutic approaches. By studying appropriate animal models, researchers can more conveniently and quickly evaluate the therapeutic effects of certain rehabilitation methods and gain deeper insights into their mechanisms. Mice, as commonly used experimental animals, have been widely employed in studies related to peripheral nerve injuries [5–7]. However, due to their small body size, current research has mainly focused on the sciatic nerve and its innervated muscles, as well as the larger muscles of the mouse forelimb and their innervating nerves [8, 9]. There is relatively little research on the intrinsic muscles of the mouse forepaw. Therefore, if mice are used as experimental animals to explore interventions that promote functional recovery of the intrinsic

CONTACT Su Jiang oscarjiangsu@126.com Department of Hand Surgery, Huashan Hospital, 12 Middle Wulumuqi Road, Shanghai 200040, China

muscles of the forepaw after ulnar nerve injury, it is first necessary to conduct a detailed study of the anatomical structure of the intrinsic muscles of the mouse forepaw. Therefore, characterizing the muscle fiber type composition is crucial, as different fiber types (e.g. slow-twitch vs. fast-twitch) exhibit distinct metabolic properties, fatigue resistance, and regenerative capacities, all of which influence functional recovery and response to rehabilitation [10]. Equally important is the analysis of neuromuscular junctions (NMJs), which serve as the key interface for neural control of muscle contraction. The structural integrity and plasticity of NMJs directly affect reinnervation success and motor relearning after nerve injury. We transected the median nerve in the upper arm of mice to induce median nerve denervation, thereby revealing the innervation territory of the ulnar nerve in the lumbrical and interosseous muscles. Recent studies demonstrated that both single or fatigue-resistant tetanic contractions of muscles can be successfully induced using electrical stimulation or optogenetic stimulation with different parameters [11, 12]. Therefore, we believe that a precise understanding of the innervation patterns and muscle fiber composition of these small intrinsic muscles may, in the future, inform the development of advanced neuroengineering strategies – such as brain–computer interfaces (BCIs) or neural interfaces [13, 14] – aimed at restoring neuromuscular function in patients with peripheral nerve injuries. Specifically, muscle groups predominantly composed of fast-twitch fibers may require stimulation parameters optimized for rapid force generation, while areas dominated by slow-twitch fibers might be better suited to long-term, low-intensity stimulation strategies for maintaining fine postural control. Furthermore, nerve transfer surgery has been shown to potentially alter the muscle fiber composition of the target muscles [15], suggesting that different donor nerves could necessitate tailored stimulation parameters to achieve effective control of the intrinsic hand muscles. Thus, the murine model data provided by this study establish a critical anatomical foundation for testing refined control algorithms based on specific muscle activation in preclinical models. While such applications remain long-term goals, establishing a solid anatomical and functional foundation in animal models is a critical first step toward enabling targeted neuromodulation or muscle reinnervation therapies. Therefore, this study seeks to fill this gap by characterizing the neural and histological basis of intrinsic forepaw muscle function in mice.

The lumbrical and interosseous muscles are important components of the intrinsic hand muscles. This study aims to use anatomical and immunohistochemical analysis to elucidate the innervation of the lumbrical and interosseous muscles by the ulnar nerve in mice, as well as their muscle fiber composition. These findings will provide an anatomical and histological basis for therapeutic interventions aimed at restoring the function of intrinsic hand muscles after ulnar nerve injury.

Materials and methods

Animals

Twenty-four male C57 mice aged 6 weeks were used for the experiment. Among 24 mice, 12 mice were used for anatomical studies of the lumbrical and interosseous muscles, six mice were used for NMJ immunofluorescence staining of the lumbrical and interosseous muscles, and six mice were used for muscle fiber immunofluorescence staining of the lumbrical and interosseous muscles.

Median nerve transection

In six out of 24 mice, the median nerve in the right upper arm segment of the mouse was exposed, and a 3 mm segment of the median nerve was excised at the midpoint of the upper arm; these six mice were used for immunofluorescence staining of the NMJ. Six months after model establishment, the mice were euthanized, and the affected-side lumbrical and interosseous muscles were harvested. The remaining 18 mice out of the 24 were euthanized at the same time as the model mice.

Dissection

In 12 out of the 24 mice, the right upper limb was harvested after euthanasia. Following fixation in 4% formaldehyde, the skin and subcutaneous tissue were incised at the distal forearm under a stereomicroscope. The ulnar nerve was then exposed, and its branches were bluntly dissected along their course until reaching the muscle entry points.

Tissue preparation

All lumbrical muscles and dorsal interosseous muscles (DIM) were dissected intact between the distal and proximal end points under a surgical microscope.

Immunofluorescence staining

To illustrate the various types of muscle fibers, we applied immunofluorescence labeling to the aforementioned cross-sections using a method adapted from prior research [16]. The tissue sections were treated overnight at 4°C with a blend of primary antibodies targeting distinct myosin heavy chain (MHC) isoforms: anti-MHC-I (BA-F8, mouse IgG2B; sourced from the Developmental Studies Hybridoma Bank [DSHB]) at a dilution of 1:100, anti-MHC-IIa (SC-71, mouse IgG1; DSHB) at 1:600, and anti-MHC-IIb (BF-F3, mouse IgM; DSHB) at 1:200. Subsequently, on the following day, these sections underwent a 4-h incubation in secondary antibodies, including Alexa Fluor 633-conjugated goat anti-mouse IgG2B (Invitrogen, Eugene, WA) at 1:250, Alexa Fluor 488-conjugated goat anti-mouse IgG1 (Invitrogen) at 1:250, and Alexa Fluor 555-conjugated goat anti-mouse IgM (Invitrogen) also at 1:250.

According to methods used in prior studies [17], the longitudinal sections were incubated at room temperature for 1 h with Alexa Fluor 488 conjugated α-bungarotoxin (Invitrogen) at a dilution of 1:500 to visualize nicotinic acetylcholine receptors on the postsynaptic membrane.

Imaging and analysis of muscle fibers and endplates

Muscle fiber type composition and identified endplate images were captured using an Olympus Fluoview confocal microscope (10× and 20× objectives; Olympus, Tokyo, Japan) equipped with three laser lines. Following a previously established method, NMJ images were presented as single-plane projections of Z-stack images with 1.0-μm spacing. Both muscle fibers and endplates were quantified using ImageJ software (developed by Wayne Rasband at NIH, Bethesda, MD, and freely accessible at rsbweb.nih.gov).

Statistical analysis

F-Statistical analyses were performed using GraphPad Prism 9 (GraphPad Software). Data are presented as mean ± standard error of the mean (SEM). Normality was assessed using the Kolmogorov–Smirnov

test. Based on the results, parametric tests were applied assuming normal distribution. Comparisons between two groups were conducted using an unpaired Student's t-test. For multiple group comparisons, one-way Analysis of variance (ANOVA) followed by Dunnett's post hoc test was used. $P < 0.05$ considered statistically significant.

Ethics

Ethical approval was granted by the Animal Ethics Committee of Fudan University.

Results

Lumbrical and interosseous muscles anatomy

The lumbrical muscles of the mouse forepaw are located on the palmar side of the forepaw and include four muscles: the first, second, third, and fourth lumbricals (Figure 1A). Each lumbrical muscle has a slender, spindle-like shape, originating from the palmar side of the flexor digitorum profundus tendon and running along the radial side of the deep and superficial flexor tendons of each digit. The first to fourth lumbrical muscles insert at the radial side of the proximal phalanges of the second to fifth digits, respectively. The muscle fiber orientation of each lumbrical aligns with the overall direction of the muscle belly, and the digital nerves run closely along the palmar side of their corresponding lumbrical muscles.

The interosseous muscles of the mouse forepaw are divided into palmar and DIMs; there are three palmar interosseous muscles and four DIMs (Figure 1B). The three palmar interosseous muscles each originate from the palmar surface of the corresponding metacarpal base, with their tendons inserting into the ulnar aspect of the second proximal phalanx, and the radial aspects of the fourth and fifth proximal phalanges, respectively. All four DIMs arise from the palmar aspects of the metacarpal bases and terminate at the proximal ends of the corresponding proximal phalanges. The muscle fibers of the interosseous muscles are arranged in a pennate distribution.

Ulnar nerve innervation of the lumbrical and interosseous muscles

The ulnar nerve contributes to the innervation of both the lumbrical and interosseous muscles of the hand (Figure 2B, C). After entering the forepaw, the ulnar nerve emits branches to innervate the third and fourth lumbrical muscles, the hypothenar muscle group, and the adductor pollicis (Figure 2A, B). Another branch descends deeper, emits muscular branches to innervate all the interosseous muscles (Figure 2C).

Immunofluorescence staining and statistical analysis of neuromuscular junction in the lumbrical and interosseous muscles

In Figure 3, we observed anatomical communication between the ulnar nerve and the median nerve in the forepaw in four of the 12 cases, indicating that the ulnar nerve and the median nerve might both contribute in the innervation of lumbrical and interosseous muscles. However, the exact proportion of these muscles innervated by the ulnar nerve, as well as which specific muscles or muscle regions are exclusively innervated by it, remains unclear. In mice, the area of motor endplates (MEPs) significantly decreases within 2 months after denervation [18]. To examine the innervation pattern of the lumbrical and interosseous muscles by the ulnar nerve, we transected the median nerve in the upper arm of mice. Six months later, the MEPs innervated by the median nerve were significantly reduced in size, allowing us to visualize the distinct innervation territory of the ulnar nerve.

Six months after median nerve transection, the average MEP area of the affected side LM1 was 16.600 ± 1.126 μm^2, which was significantly smaller than that of the contralateral unaffected side (138.700 ± 8.515 μm^2) (Figure 4A, E). Similarly, the average MEP area of the affected side LM2 was significantly reduced at 13.970 ± 1.185 μm^2 compared to the unaffected side (141.400 ± 7.211 μm^2) (Figure 4B, E).

For LM3, the average MEP area on the injured side measured 42.140 ± 5.382 μm^2, which was also significantly lower than the corresponding value on the unaffected side (142.800 ± 5.873 μm^2). However, this value was notably higher compared to those observed in both LM1 and LM2 on the affected side (Figure 4C, E).

In contrast, the average MEP area of the affected side LM4 was 152.200 ± 10.63 μm^2, which did not show any statistically significant difference when compared to the unaffected side (153.800 ± 2.194 μm^2), indicating the preservation of NMJ morphology in this region (Figure 4D, E).

For the interosseous muscles, we representatively selected all the DIMs as the target muscles. Six months after median nerve transection, the average MEP areas of the affected side DIM1, DIM2, DIM3, and DIM4 in mice were 137.300 ± 6.199 μm^2, 157.400 ± 4.050 μm^2, 171.100

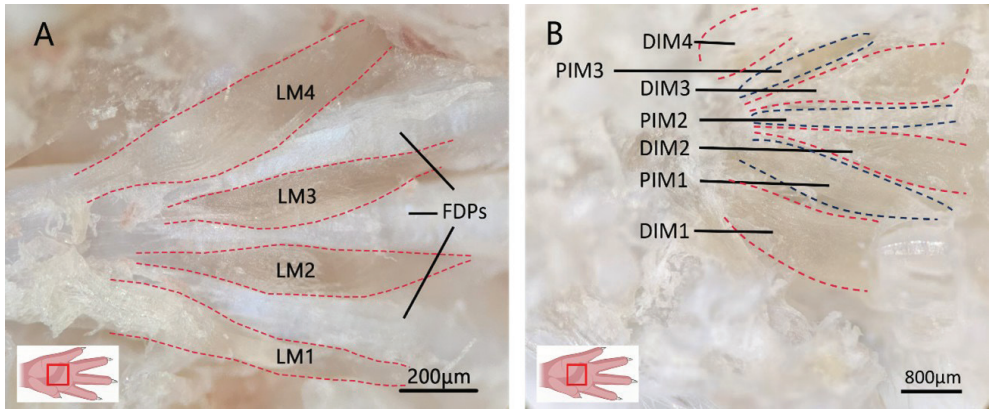

Figure 1. Lumbrical and interosseous muscles of the mouse forepaw. (A) Anatomical location of the lumbrical muscles. Scale bar = 200 μm. (B) Anatomical location of the interosseous muscles. Scale bar = 800 μm. LM: lumbrical muscle; FDP: Flexor digitorum profundus tendon; PIM: palmar interosseus muscle; DIM: dorsal interosseus muscle.

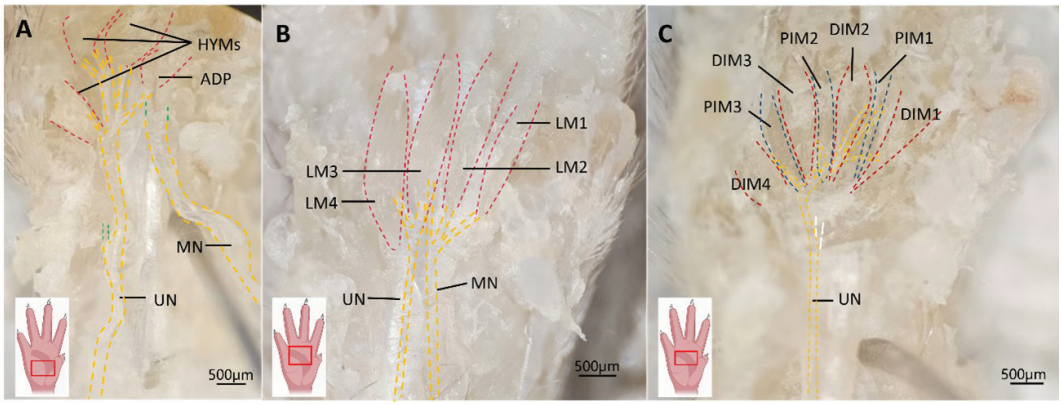

Figure 2. Illustration of the ulnar nerve's distribution to the intrinsic hand muscles. (A) Superficial structures. The hypothenar muscles are elevated to expose the underlying structures. Green dashed lines indicate the nerve passing beneath the muscle. HYMs: Hypothenar muscles; ADP: Adductor pollicis; UN: ulnar nerve; MN: median nerve. Scale bar = 500 μm. (B) The innervation of the lumbrical muscles by the ulnar nerve. LM: lumbrical muscle; UN: ulnar nerve. (C) The innervation of the interosseous muscles by the ulnar nerve. White dashed line indicates a transected nerve, revealing deeper anatomical features. PIM: Palmar interosseous muscles; DIM: Dorsal interosseous muscles. Scale bar = 500 μm. The image in the lower-left corner indicates the direction of the mouse paw.

± 10.380 μm^2, and 143.400 ± 7.272 μm^2, respectively, showing no significant difference compared to the unaffected side (DIM1, 142.500 ± 8.186 μm^2. DIM2, 153.200 ± 10.130 μm^2. DIM3, 140.500 ± 9.978 μm^2, and DIM4, 131.300 ± 5.993 μm^2) (Figure 4F–J).

Immunofluorescence staining and statistical analysis of muscle fibers in the lumbrical and interosseous muscles

Understanding the composition and relative proportion of muscle fiber types is crucial for elucidating their functional roles and response to neuromuscular disorders. Taking the third DIM and the fourth lumbrical muscle – two muscles predominantly innervated by the ulnar nerve – as examples, we used muscle fiber immunofluorescence to characterize the muscle fiber types in the lumbrical and interosseous muscles under normal innervation by the ulnar nerve.

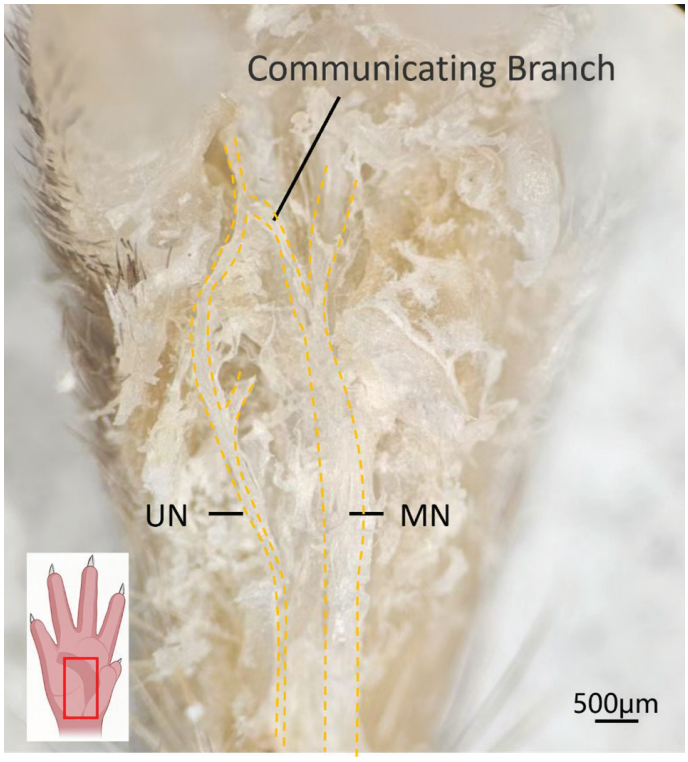

Figure 3. Communication between the ulnar and median nerves. The image in the lower-left corner indicates the direction of the mouse paw. UN: ulnar nerve; MN: median nerve. Scale bar = 500 μm.

The fiber number percentages of MHC-I, IIa, and IIb muscle fibers in the fourth lumbrical muscle of the mouse were 3.89% ± 1.10%, 31.67% ± 7.31%, and 64.44% ± 7.17%, respectively (Figure 5A, C). In comparison, the third interosseous muscle displayed a distinct fiber type composition, with MHC-I, IIa, and IIb fiber percentages measuring 11.45% ± 1.92%, 88.55% ± 1.92%, and 0%, respectively (Figure 5B, D).

The average cross-sectional areas of MHC-I, IIa, and IIb muscle fibers in the fourth lumbrical muscle of the mouse were measured at 118.1 ± 14.43 μm^2, 237.1 ± 21.51 μm^2, and 327.9 ± 30.21 μm^2, respectively (Figure 5A, E). In comparison, in the third interosseous muscle, the average cross-sectional areas were significantly larger for both MHC-I (321.6 ± 40.04 μm^2) and MHC-IIa (538.2 ± 96.38 μm^2) fibers, while no MHC-IIb fibers were detected (Figure 5B, F).

The cross-sectional area percentages of MHC-I, IIa, and IIb muscle fibers in the fourth lumbrical muscle of the mouse were 2.00% ± 0.42%, 27.04% ± 7.00%, and 70.96% ± 7.16%, respectively (Figure 5A, G). In contrast, the third interosseous muscle exhibited a markedly different distribution, with MHC-I, IIa, and IIb fiber area percentages measuring 8.21% ± 1.76%, 91.79% ± 1.76%, and 0%, respectively (Figure 5B, H).

Discussion

The ulnar nerve, one of the main branches of the brachial plexus, plays a crucial role in innervating the intrinsic hand muscles responsible for fine motor functions. Ulnar nerve injury is one of the most common types of peripheral nerve injuries encountered clinically. After injury, both the motor function of the target muscles and the sensory function of the skin innervated by the nerve distal to the injured site are affected [19]. Compared with median and radial nerve injuries, the recovery of motor function in the affected limb following ulnar nerve repair tends to be less satisfactory [20]. Particularly in cases of high-level ulnar nerve injury, although early surgical repair may restore partial sensory function over time, effective recovery of the intrinsic hand muscle function remains challenging [21]. This significantly impacts the patient's quality of life.

To address the critical clinical issue of poor recovery of distal target muscles following ulnar nerve injury, more experimental research is

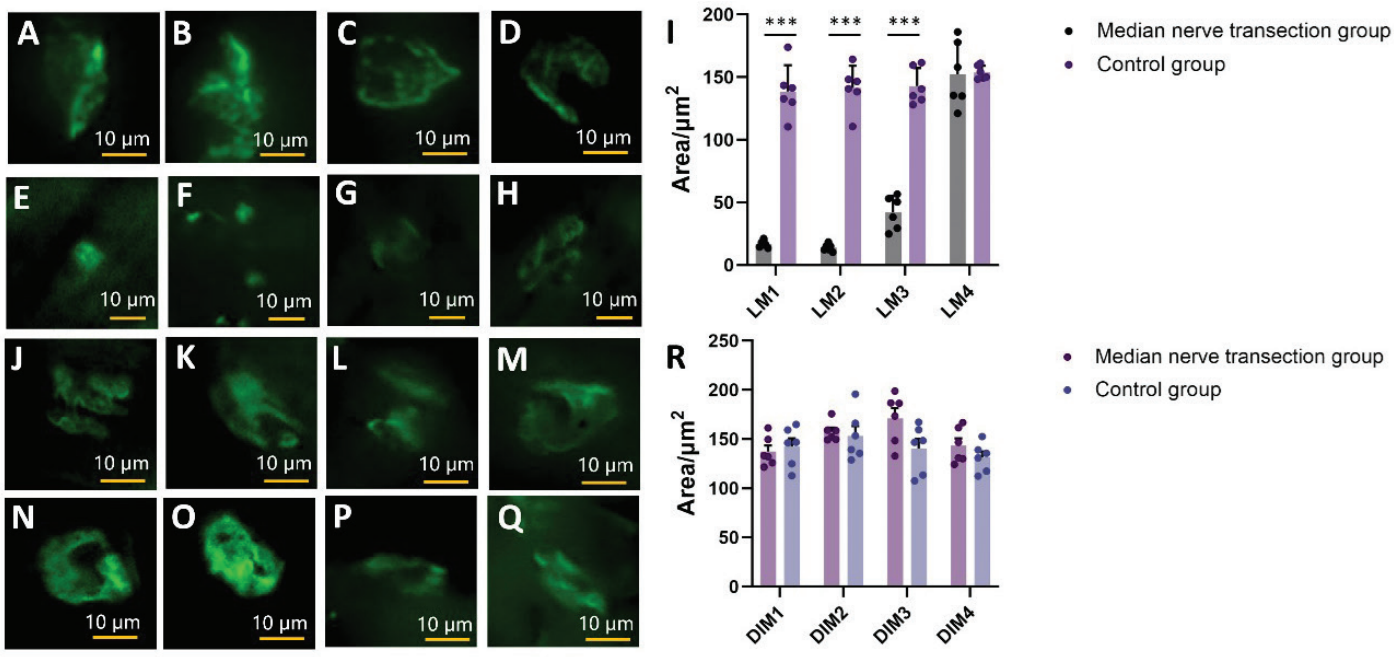

Figure 4. Immunofluorescence Staining of neuromuscular junction in the Lumbrical and Interosseous Muscles. (A–D) Immunofluorescence images of NMJs in the first lumbrical muscle (A), the second lumbrical muscle (B), the third lumbrical muscle (C) and the fourth lumbrical muscle (D) in normal mice. The NMJs is intact. Scale bar = 10 μm. E-H. Immunofluorescence images of NMJs in the first lumbrical muscle (E), the second lumbrical muscle (F), the third lumbrical muscle (G) and the fourth lumbrical muscle (H) at 6 months after median nerve transection. The NMJs is fragmented. Scale bar = 10 μm. I. Statistical comparison of immunofluorescence images of NMJs in the first, second, third, and fourth lumbrical muscles between the healthy and affected sides at 6 months after median nerve transection. J-M. Immunofluorescence images of NMJs in the first dorsal interosseous muscles (J), the second dorsal interosseous muscles (K), the third dorsal interosseous muscles (L) and the fourth dorsal interosseous muscles (M) in normal mice. The NMJs is intact. Scale bar = 10 μm. N-Q. Immunofluorescence images of NMJs in the first dorsal interosseous muscles (N), the second dorsal interosseous muscles (O), the third dorsal interosseous muscles (P) and the fourth dorsal interosseous muscles (Q) at 6 months after median nerve transection. The NMJs is intact. Scale bar = 10 μm. R. Statistical comparison of immunofluorescence images of NMJs in the first, second, third, and fourth dorsal interosseous muscles between the healthy and affected sides at 6 months after median nerve transection. All data are presented as mean ± SEM. ***$P < 0.001$.

needed to explore and optimize appropriate treatment and rehabilitation techniques. Conducting studies in animal models allows for relatively rapid and straightforward data collection, providing a foundation for the subsequent clinical application of these techniques. Mice are an accessible and cost-effective experimental animal, requiring minimal housing space, and are widely used in various research fields. While researchers have extensively studied peripheral nerve injury and repair in mice, most of this work has focused on the sciatic nerve in the hindlimb [9]. Therefore, to investigate the recovery of intrinsic hand muscle function after ulnar nerve injury, it is necessary to develop and utilize a targeted model of ulnar nerve injury.

Before confirming the use of mice as a model to study the recovery of intrinsic hand muscle function after ulnar nerve injury, it is essential to clarify the similarities and differences between mice and humans regarding the ulnar nerve and its target muscles. Currently, there is limited research on the anatomy of the mouse forelimb. Mathewson et al. investigated the anatomical structure of 22 muscles in the mouse forelimb but did not examine the intrinsic muscles of the mouse forepaw [22]. Therefore, conducting an anatomical study of the intrinsic muscles of the mouse forepaw is the first step in selecting mice as a model for ulnar nerve injury. Simultaneously, it is necessary to determine which muscle or muscles should be selected for evaluation following ulnar nerve repair. In humans, the lumbrical and interosseous muscles are two critical components of the intrinsic hand muscles. The lumbrical muscles function to flex the metacarpophalangeal joints and extend the interphalangeal joints, while the interosseous muscles are responsible for finger abduction and adduction. These functions are indispensable for fine motor control of the human hand. In summary, we have chosen the lumbrical and interosseous muscles of the mouse as the target muscles for evaluation after ulnar nerve repair. Our study found that the lumbrical muscles of the mouse forepaw include four muscles, and there are three palmar interosseous muscles and four DIMs. Rinker et al. described that the forepaw of the rodent Sigmodon possesses seven interosseous muscles, which is in agreement with our findings [23].

In humans, the ulnar nerve innervates all interosseous muscles [24]. The fourth lumbrical muscle in humans is innervated by the ulnar nerve, while the innervation pattern of the third lumbrical muscles varies: some are solely innervated by the median nerve, some by both the median and ulnar nerves, and others exclusively by the ulnar nerve [25, 26]. Through anatomical studies, we have found that the ulnar nerve of mice innervates the third and fourth lumbrical muscles and all interosseous muscles, which is similar to humans (Figure 6A, B).

The anatomical variations of communicating branches (CBs) between the ulnar and median nerves in the hand have been well-characterized in human studies, providing critical insights for understanding potential functional implications and surgical risks. Loukas et al. documented CBs in 85% (170/200) of cadaveric hands, classifying them into four major types: Type I (84.1%) originating from the ulnar nerve to join the median nerve distally, Type II (7.1%) arising from the median nerve to merge with the ulnar nerve, Type III (3.5%)

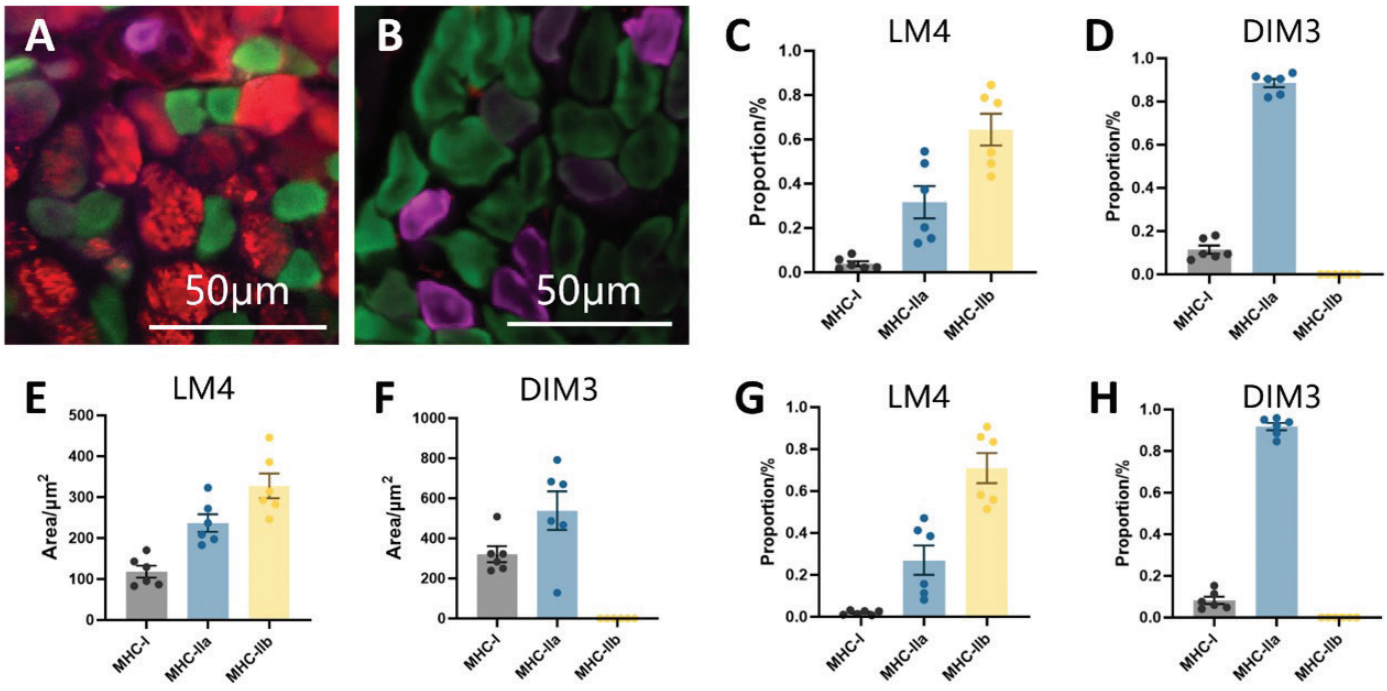

Figure 5. Immunofluorescence Staining of Muscle Fibers in the Lumbrical and Interosseous Muscles. (A) Immunofluorescence staining image of the fourth lumbrical muscle fiber in the mouse forepaw. Purple: MHC-I type muscle fibers. Green: MHC-IIa type muscle fibers. Red: MHC-IIb type muscle fibers. Scale bar = 50 μm. (B) Immunofluorescence staining image of the third dorsal interosseous muscle fiber in the mouse forepaw. Purple: MHC-I type muscle fibers. Green: MHC-IIa type muscle fibers. Scale bar = 50 μm. (C, D) Statistics of the proportion of different types of muscle fibers in the third dorsal interosseous muscle (C) and fourth lumbrical muscle (D) in the mouse forepaw. (E, F) Statistics of the average area of different types of muscle fibers in the third dorsal interosseous muscle (E) and fourth lumbrical muscle (F) in the mouse forepaw. GH. Statistics of the area proportion of different types of muscle fibers in the third dorsal interosseous muscle (G) and fourth lumbrical muscle of the mouse forepaw (H). All data are presented as mean ± SEM.

with perpendicular course lacking a defined origin, and Type IV (5.3%) as mixed multi-branch patterns [27]. Morphometric analysis revealed that 83% of CBs resided in a 'risk area' spanning 35%–62% of the distance between the bisstyloid line and metacarpophalangeal joint line, highlighting susceptibility to iatrogenic injury during carpal tunnel release [27]. Anatomical stratification shows superficial CBs (e.g. Berrettini branch) lie deep to the superficial palmar arch, connecting the third and fourth common digital nerves, while deep CBs (16% prevalence) originate from the deep ulnar nerve, traverse posterior to flexor tendons, and join the median nerve near the pisiform bone and adductor pollicis muscle [28, 29]. Clinically, these CBs may mediate sensory overlap – for instance, ulnar-to-median communication can preserve sensation in the middle/ring fingers after median nerve injury, potentially misleading diagnostic assessments [27]. Case reports have shown reduced ring finger sensation post-carpal tunnel release due to CB injury, reinforcing their functional significance [30]. Notably, high-resolution sonography has enabled non-invasive visualization of superficial CBs, with 100% ultrasound detectability in cadaveric hands, aiding preoperative localization to minimize surgical trauma [31]. Rare variations, such as a forearm-originating ulnar-to-median CB merging with the median nerve distal to the flexor retinaculum, have also been described [32], underscoring the spectrum of anatomical diversity. Current knowledge is predominantly human-focused, with limited data on rodent CBs. Future studies integrating microdissection and electrophysiology in mouse forepaws could provide a systematic characterization of CBs and their role in motor innervation of intrinsic hand muscles, potentially bridging gaps in translational neuroanatomy. Our study has revealed the presence of CBs between the ulnar and median nerves in the mouse forepaw, which is similar to what is observed in humans. This finding underscores the suitability of mice as an appropriate animal model for studying the innervation and function of intrinsic hand muscles.

Muscle contraction is regulated at the NMJ, a peripheral synapse consisting of a motor nerve terminal, specialized muscle structures, and non-myelinating terminal Schwann cells [33, 34]. A defining feature of the mammalian NMJ is the high-density clustering and maintenance of nicotinic acetylcholine receptors (AChRs) in the postsynaptic membrane [35]. The typical and mature morphology of the NMJ is often described as having a 'pretzel-like' structure [36]. However, a common sign of NMJ alterations is postsynaptic fragmentation. Specifically, denervation of the MEP initiates a cascade of events, leading to a shortened half-life of AChRs in the postsynaptic membrane, reduced postsynaptic density, and eventual loss of postsynaptic regions [35].

In an experiment by Francisca Bermedo-García et al., they found that 7 days after denervation of the cranial levator auris longus (LAL) muscle, the postsynaptic domain underwent morphological changes, as quantification of the area of AChR aggregates (excluding ectopic aggregates) showed a progressive decrease, which was already detectable 7 days after injury [37]. Viviana Pérez et al. used an in vivo two-color BTX technique to study the dynamics of AChRs after denervation [38]. Specifically, the postsynaptic regions of LAL muscles in live mice were labeled with a non-saturating dose of fluorescently tagged BTX-1. Seven days after denervation, the muscles were excised and relabeled with another fluorescently tagged BTX-2. Using confocal microscopy, AChR aggregates were classified as 'stable' if the labeling intensities of BTX-1 and BTX-2 were similar, or as 'dynamic' if BTX-1 labeling was mostly absent and BTX-2 showed higher intensity [39]. The results showed that denervation significantly increased the proportion of dynamic AChR aggregates in the LAL muscles [39]. Using progressive tissue optical clearing technology, Yin et al. applied

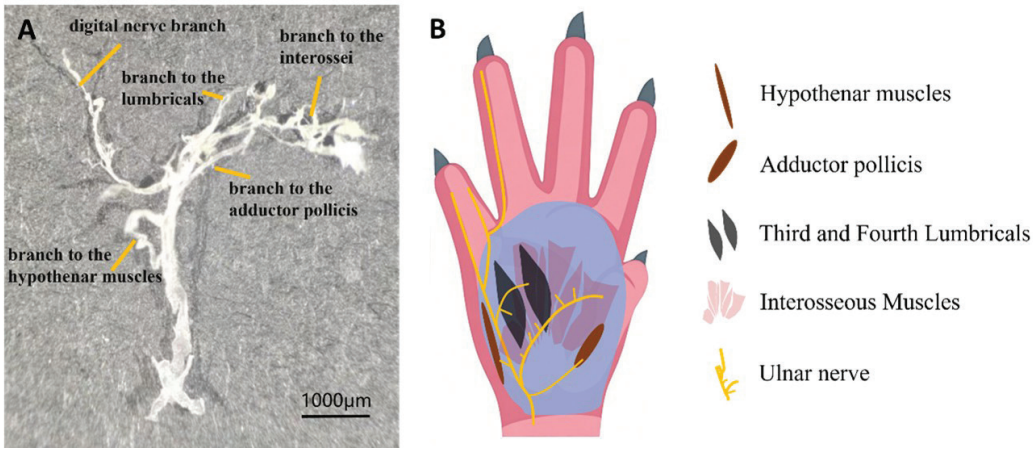

Figure 6. Ulnar nerve innervation in the hand of mice. (A) The ulnar nerve was completely harvested from the wrist distally and then photographed. Scale bar = 1,000 μm. (B) Schematic representation of ulnar nerve innervation in the hand.

3D imaging to study the spatial distribution of MEPs and their changes following denervation in mice [18]. They observed that 2 months post-denervation, the average width of MEP lamella clusters increased, while the mean volume of individual MEPs significantly decreased. This indicated that after denervation, MEPs broke down into smaller fragments along the lamella clusters until they eventually disappeared [18, 40].

The 6-month post-injury time point was selected in this study to allow sufficient time for the median nerve-innervated muscles to undergo substantial atrophy and MEP fragmentation. This extended duration enables the visualization of chronic, stable adaptations in neuromuscular organization and muscle properties. While the capacity for collateral sprouting and spontaneous reinnervation in rodent models post-transection is recognized, the functional and morphological compensation that ensues is invariably distinct from the normal state [41]. Our results are consistent with this principle, demonstrating that such compensatory reinnervation does not fully restore the native neuromuscular profile. Our experimental results showed that after median nerve transection, no intact MEPs were found in the first and second lumbrical muscles of the mouse forepaw, indicating that the ulnar nerve does not innervate these two muscles. The third lumbrical muscle exhibited both intact and fragmented MEPs, suggesting that it is innervated by both the ulnar and median nerves. The area of MEPs in the fourth lumbrical muscle showed no significant difference compared to a normal fourth lumbrical muscle, indicating that the fourth lumbrical muscle is entirely innervated by the ulnar nerve. All DIMs retained normal MEP morphology, confirming their predominant or sole innervation by the ulnar nerve. Importantly, the exclusive ulnar innervation of LM4 and the DIMs identifies them as reliable targets for evaluating functional reinnervation and therapeutic interventions.

Mammalian skeletal muscle consists of various fiber types, and the diversity among these fibers enables the same muscle to perform a range of tasks [10]. These include sustained low-intensity activities, repeated moderate contractions, and rapid, powerful maximal contractions [10]. MHC isoforms are commonly used as classification criteria and are regarded as molecular markers for fiber types [42, 43]. Under specific conditions, alterations in MHC isoform expression can be prompted [44]. According to Jakubiec-Puka et al., upon reinnervation, the soleus muscle recovered its normal MHC pattern within 10 days, with an increased proportion of type I isoform. In contrast, in the reinnervated fast muscle, the IIb/IIa ratio continued to decrease [45]. Huey et al. investigated these changes at the mRNA level [46]. In the tibialis anterior muscle, the type IIb MHC mRNA was significantly reduced by day 4 following denervation and remained decreased for up to a month. Meanwhile, type IIa mRNA increased significantly by day 7, staying elevated until day 14 before returning to control values [46]. The results of this experiment show that the lumbrical muscle is predominantly composed of Type IIa intermediate fibers and Type IIb fast-twitch fibers. In contrast, the interosseous muscle mainly consists of Type I slow-twitch fibers and Type IIa intermediate fibers, which can provide a theoretical basis for understanding the changes in fiber types of the lumbrical and interosseous muscles in mice after nerve injury.

Compelling experimental evidence demonstrates that when a target muscle is reinnervated by an alternative donor nerve, its fiber-type profile can undergo a significant shift to mirror that of the donor nerve's original musculature [15, 41]. For instance, Bergmeister et al. showed that after transferring the high-capacity ulnar nerve to the lateral head of the biceps – a muscle normally innervated by the musculocutaneous nerve – the reinnervated biceps underwent a transformation from a predominantly fast type IIb fiber population to one rich in slower, more fatigue-resistant type I and IIa fibers, characteristic of native ulnar-innervated muscles like the lumbricals [15]. Furthermore, this plasticity extends beyond somatic motor inputs; even aberrant autonomic reinnervation, as observed in denervated facial muscles, can drive a complete phenotypic switch, converting the muscle to a purely intermediate type IIa profile [41]. Together, these studies establish that any change in efferent neural drive, whether intentional through surgical nerve transfer or spontaneous via collateral sprouting, will inevitably alter the functional properties of the target muscle. Therefore, our baseline data revealing the precise, heterogeneous fiber-type signatures of the intrinsic hand muscles are not merely descriptive. They serve as a crucial physiological benchmark. Preserving or restoring this native fiber-type architecture is paramount for maintaining the delicate balance of force, speed, and endurance required for dexterous hand function.

The baseline data established in this study have significant implications for neuroengineering and the development of next-generation neural interfaces for hand function restoration. In BCIs or peripheral nerve stimulation systems, algorithms must simulate the natural contraction speeds, force profiles, and fatigue properties dictated by the underlying muscle fiber-type composition. Our quantitative characterization of MHC isoform distributions across intrinsic hand muscles provides a physiological blueprint that can be directly integrated into stimulation protocols to generate more naturalistic and fatigue-resistant grasping motions. Importantly, recent advances in implantable neurotechnology – such as our fully implantable multisite optogenetic stimulation system (FIMOSS) –

now enable long-term, sub-nerve-resolution interrogation and modulation of peripheral nerve plexuses in vivo [12]. Building on our earlier multisite optogenetic stimulation device (MOSD) [47], which demonstrated acute fascicle-specific control of forelimb movements in mice, FIMOSS offers a powerful platform for chronic electrophysiological and behavioral studies following nerve injury or reconstructive surgery [12]. By combining our anatomical and fiber-type mapping with such high-precision neuromodulation tools, future neuroprosthetic strategies can be tailored not only to target specific motor fascicles but also to deliver stimulation patterns calibrated to the contractile phenotype of their innervated muscles – thereby enhancing functional fidelity in ulnar-territory reanimation and beyond.

In conclusion, we have studied the innervation of the lumbrical and interosseous muscles of the mouse forepaw by the ulnar nerve, as well as the muscle fiber types of the third DIM and fourth lumbrical muscle, which are innervated by the ulnar nerve. This study did not investigate the pathological changes following ulnar nerve injury. In future research, we will further explore nerve regeneration and the recovery of intrinsic hand muscle function after ulnar nerve injury in mice, using the fully implantable optoelectronic stimulation system we have developed.

Acknowledgments

We would like to express our sincere gratitude to Dr. Chunmin Liang, Dr. Biao Yan and Dr. Fei Wang for their valuable suggestions on experimental design and data interpretation. Special thanks go to Dr. Jifeng Li and Dr. Jing Rui, whose support during the experimental phase was instrumental in the successful completion of this work.

Disclosure statement

The authors declare that they have no conflict of interest.

Funding

This work was supported by the STI 2030-Major Projects [grant number 2022ZD0208605, 2022ZD0208600]; National Natural Science Foundation of China [grant number 82072545]; Science and Technology Innovation Plan of Shanghai Science and Technology Commission [grant number 22S31902100]; Shanghai Municipal Key Clinical Specialty [grant number shslczdzk05601]; Shanghai Key Laboratory of Peripheral Nerve and Microsurgery [grant number 20DZ2270200].

References

[1] Lee SK, Wisser JR. Restoration of pinch in intrinsic muscles of the hand. Hand Clin. 2012;28(1):45–51. https://doi.org/10.1016/j.hcl.2011.10.002

[2] Dell PC, Sforzo CR. Ulnar intrinsic anatomy and dysfunction. J Hand Ther. 2005;18(2):198–207. https://doi.org/10.1197/j.jht.2005.02.008

[3] Vordemvenne T, Langer M, Ochman S, et al. Long-term results after primary microsurgical repair of ulnar and median nerve injuries: a comparison of common score systems. Clin Neurol Neurosurg. 2007;109(3):263–271. https://doi.org/10.1016/j.clineuro.2006.11.006

[4] Ruijs ACJ, Jaquet J-B, Kalmijn S, et al. Median and ulnar nerve injuries: a meta-analysis of predictors of motor and sensory recovery after modern microsurgical nerve repair. Plast Reconstr Surg. 2005;116(2):484. https://doi.org/10.1097/01.prs.0000172896.86594.07

[5] Mehrotra P, Jablonski J, Toftegaard J, et al. Skeletal muscle reprogramming enhances reinnervation after peripheral nerve injury. Nat Commun. 2024;15(1):9218. https://doi.org/10.1038/s41467-024-53276-4

[6] Zhong K, Huang Y, Zilundu PLM, et al. Motor neuron survival is associated with reduced neuroinflammation and increased autophagy after brachial plexus avulsion injury in aldose reductase-deficient mice. J Neuroinflammation. 2022;19(1):271. https://doi.org/10.1186/s12974-022-02632-6

[7] Li M, Xu J, Zou Y, et al. Motor neuron-specific RhoA knockout delays degeneration and promotes regeneration of dendrites in spinal ventral horn after brachial plexus injury. Neural Regen Res. 2023;18(12):2757–2761. https://doi.org/10.4103/1673-5374.373657

[8] Nikolaou S, Hu L, Cornwall R. Afferent innervation, muscle spindles, and contractures following neonatal brachial plexus injury in a mouse model. J Hand Surg. 2015;40(10):2007–2016. https://doi.org/10.1016/j.jhsa.2015.07.008

[9] Jha MK, Passero JV, Rawat A, et al. Macrophage monocarboxylate transporter 1 promotes peripheral nerve regeneration after injury in mice. J Clin Investig. 2021;131(21):e141964. https://doi.org/10.1172/JCI141964

[10] Schiaffino S, Reggiani C. Fiber types in mammalian skeletal muscles. Physiol Rev Am Physiol Soc. 2011;91(4):1447–1531. https://doi.org/10.1152/physrev.00031.2010

[11] Herrera-Arcos G, Song H, Yeon SH, et al. Closed-loop optogenetic neuromodulation enables high-fidelity fatigue-resistant muscle control. Sci Robot. 2024;9(90):eadi8995. https://doi.org/10.1126/scirobotics.adi8995

[12] Zhou M, Yan B, Yang F, et al. A wireless optogenetic stimulation system for long-term function evaluation of mice forelimb with sub-nerve resolution. Nat Commun. 2025;16(1):8702. https://doi.org/10.1038/s41467-025-63746-y

[13] Ajiboye AB, Willett FR, Young DR, et al. Restoration of reaching and grasping in a person with tetraplegia through brain-controlled muscle stimulation: a proof-of-concept demonstration. Lancet. 2017;389(10081):1821–1830. https://doi.org/10.1016/S0140-6736(17)30601-3

[14] Dong C, Carnicer-Lombarte A, Bonafè F, et al. Electrochemically actuated microelectrodes for minimally invasive peripheral nerve interfaces. Nat Mater. 2024;23(7):969–976. https://doi.org/10.1038/s41563-024-01886-0

[15] Bergmeister KD, Aman M, Muceli S, et al. Peripheral nerve transfers change target muscle structure and function. Sci Adv. 2019;5(1):eaau2956. https://doi.org/10.1126/sciadv.aau2956

[16] Prukop T, Wernick S, Boussicault L, et al. Synergistic PXT3003 therapy uncouples neuromuscular function from dysmyelination in male Charcot–Marie–Tooth disease type 1A (CMT1A) rats. J Neurosci Res. 2020;98(10):1933–1952. https://doi.org/10.1002/jnr.24679

[17] Roy A, Kumar A. Supraphysiological activation of TAK1 promotes skeletal muscle growth and mitigates neurogenic atrophy. Nat Commun. 2022;13(1):2201. https://doi.org/10.1038/s41467-022-29752-0

[18] Yin X, Yu T, Chen B, et al. Spatial distribution of motor endplates and its adaptive change in skeletal muscle. Theranostics. 2019;9(3):734–746. https://doi.org/10.7150/thno.28729

[19] Basar H, Basar B, Erol B, et al. Comparison of ulnar nerve repair according to injury level and type. Int Orthop. 2014;38(10):2123–2128. https://doi.org/10.1007/s00264-014-2430-y

[20] Murovic JA. Upper-extremity peripheral nerve injuries: a Louisiana State University Health Sciences Center literature review with comparison of the operative outcomes of 1837 Louisiana State University Health Sciences Center median,

radial, and ulnar nerve lesions. Neurosurgery. 2009;65(4 Suppl): A11–A17. https://doi.org/10.1227/01.NEU.0000339130.90379.89
[21] Sallam AA, El-Deeb MS, Imam MA. Nerve transfer versus nerve graft for reconstruction of high ulnar nerve injuries. J Hand Surg. 2017;42(4):265–273. https://doi.org/10.1016/j.jhsa.2017.01.027
[22] Mathewson MA, Chapman MA, Hentzen ER, et al. Anatomical, architectural, and biochemical diversity of the murine forelimb muscles. J Anat. 2012;221(5):443–451. https://doi.org/10.1111/j.1469-7580.2012.01559.x
[23] Rinker GC. The comparative myology of the mammalian genera Sigmodon, Oryzomys, Neotoma, and Peromyscus (Cricetinae), with remarks on their intergeneric relationships. Ann Arbor: University of Michigan Museum of Zoology; 1954.
[24] Yang T, Rui Y-J. Innervation of the lumbrical and interosseous muscles in hand: analysis of distribution of nerve fascicles and quantification of their surface projections. J Plast Surg Hand Surg. 2022;56(5):310–317. https://doi.org/10.1080/2000656X.2021.1981348
[25] Chim H, Shekouhi R, Ahmed SH, et al. Anatomical characterization of the motor branch to the fourth lumbrical: a cadaver study. J Hand Surg Am. 2025;50(11):1401.e1-1401.e7.
[26] Zoghi M, Pearce SL, Nordstrom MA. Differential modulation of intracortical inhibition in human motor cortex during selective activation of an intrinsic hand muscle. J Physiol. 2003;550(Pt 3):933–946. https://doi.org/10.1113/jphysiol.2003.042606
[27] Loukas M, Louis RG, Stewart L, et al. The surgical anatomy of ulnar and median nerve communications in the palmar surface of the hand. J Neurosurg. 2007;106(5):887–893. https://doi.org/10.3171/jns.2007.106.5.887
[28] Meals RA, Shaner M. Variations in digital sensory patterns: a study of the ulnar nerve-median nerve palmar communicating branch. J Hand Surg. 1983;8(4):411–414. https://doi.org/10.1016/S0363-5023(83)80200-7
[29] Loukas M, Bellary SS, Tubbs RS, et al. Deep palmar communications between the ulnar and median nerves. Clin Anat. 2011;24(2):197–201. https://doi.org/10.1002/ca.21093
[30] May JW, Rosen H. Division of the sensory ramus communicans between the ulnar and median nerves: a complication following carpal tunnel release. A case report. J Bone Joint Surg Am. 1981;63(5):836–838. https://doi.org/10.2106/00004623-198163050-00025
[31] Dukan R, Otayek S, Pierrart J, et al. High-resolution sonographic study of the communicating branch of Berrettini: an anatomical feasibility study. J Hand Surg Eur Vol. 2021;46(7):738–742. https://doi.org/10.1177/1753193421999638
[32] Hoogbergen MM, Kauer JM. An unusual ulnar nerve-median nerve communicating branch. J Anat. 1992;181(Pt 3):513–516.
[33] Slater CR. The functional organization of motor nerve terminals. Progr Neurobiol. 2015;134:55–103. https://doi.org/10.1016/j.pneurobio.2015.09.004
[34] Sanes JR, Lichtman JW. Development of the vertebrate neuromuscular junction. Annu Rev Neurosci. 1999;22:389–442. https://doi.org/10.1146/annurev.neuro.22.1.389
[35] Martinez-Pena Y, Valenzuela I, Akaaboune M. The metabolic stability of the nicotinic acetylcholine receptor at the neuromuscular junction. Cells. 2021;10(2):358. https://doi.org/10.3390/cells10020358
[36] Koppel N, Friese MB, Cardasis HL, et al. Vezatin is required for the maturation of the neuromuscular synapse. Mol Biol Cell. 2019;30(20):2571–2583. https://doi.org/10.1091/mbc.E19-06-0313
[37] Bermedo-García F, Zelada D, Martínez E, et al. Functional regeneration of the murine neuromuscular synapse relies on long-lasting morphological adaptations. BMC Biol. 2022;20:158. https://doi.org/10.1186/s12915-022-01358-4
[38] Haddix SG, Lee YI, Kornegay JN, et al. Cycles of myofiber degeneration and regeneration lead to remodeling of the neuromuscular junction in two mammalian models of Duchenne muscular dystrophy. PLoS One. 2018;13(10):e0205926. https://doi.org/10.1371/journal.pone.0205926
[39] Pérez V, Bermedo-Garcia F, Zelada D, et al. The p75NTR neurotrophin receptor is required to organize the mature neuromuscular synapse by regulating synaptic vesicle availability. Acta Neuropathol Commun. 2019;7:147. https://doi.org/10.1186/s40478-019-0802-7
[40] Huang X, Jiang J, Xu J. Denervation-related neuromuscular junction changes: from degeneration to regeneration. Front Mol Neurosci. 2022;14:810919. https://doi.org/10.3389/fnmol.2021.810919
[41] Tereshenko V, Dotzauer DC, Luft M, et al. Autonomic nerve fibers aberrantly reinnervate denervated facial muscles and alter muscle fiber population. J Neurosci. 2022;42(44):8297–8307. https://doi.org/10.1523/JNEUROSCI.0670-22.2022
[42] Larsson L, Moss RL. Maximum velocity of shortening in relation to myosin isoform composition in single fibres from human skeletal muscles. J Physiol. 1993;472:595–614. https://doi.org/10.1113/jphysiol.1993.sp019964
[43] Qaisar R, Bhaskaran S, Van Remmen H. Muscle fiber type diversification during exercise and regeneration. Free Radic Biol Med. 2016;98:56–67.
[44] Pette D, Staron RS. Myosin isoforms, muscle fiber types, and transitions. Microsc Res Tech. 2000;50(6):500–509. https://doi.org/10.1002/1097-0029(20000915)50:6<500::AID-JEMT7>3.0.CO;2-7
[45] Jakubiec-Puka A, Kordowska J, Catani C, et al. Myosin heavy chain isoform composition in striated muscle after denervation and self-reinnervation. Eur J Biochem. 1990;193(3):623–628. https://doi.org/10.1111/j.1432-1033.1990.tb19379.x
[46] Huey KA, Bodine SC. Changes in myosin mRNA and protein expression in denervated rat soleus and tibialis anterior. Eur J Biochem. 1998;256(1):45–50. https://doi.org/10.1046/j.1432-1327.1998.2560045.x
[47] Zheng H, Zhang Z, Jiang S, et al. A shape-memory and spiral light-emitting device for precise multisite stimulation of nerve bundles. Nat Commun. 2019;10(1):2790. https://doi.org/10.1038/s41467-019-10418-3